

## MIT Open Access Articles

*Powered Ankle-Foot Prosthesis  
Improves Walking Metabolic Economy*

The MIT Faculty has made this article openly available. *Please share* how this access benefits you. Your story matters.

**Citation:** Au, S.K., J. Weber, and H. Herr. "Powered Ankle--Foot Prosthesis Improves Walking Metabolic Economy." *Robotics, IEEE Transactions on* 25.1 (2009): 51-66. © Copyright 2009 IEEE.

**As Published:** <http://dx.doi.org/10.1109/TRO.2008.2008747>

**Publisher:** Institute of Electrical and Electronics Engineers

**Persistent URL:** <http://hdl.handle.net/1721.1/51818>

**Version:** Final published version: final published article, as it appeared in a journal, conference proceedings, or other formally published context

**Terms of Use:** Article is made available in accordance with the publisher's policy and may be subject to US copyright law. Please refer to the publisher's site for terms of use.



# Powered Ankle–Foot Prosthesis Improves Walking Metabolic Economy

Samuel K. Au, Jeff Weber, and Hugh Herr, *Member, IEEE*

**Abstract**—At moderate to fast walking speeds, the human ankle provides net positive work at high-mechanical-power output to propel the body upward and forward during the stance period. On the contrary, conventional ankle–foot prostheses exhibit a passive-elastic response during stance, and consequently, cannot provide net work. Clinical studies indicate that transtibial amputees using conventional prostheses have higher gait metabolic rates than normal. Researchers believe that the main cause for these higher rates is due to the inability of conventional prostheses to provide sufficient positive power at terminal stance in the trailing leg to limit heel strike losses of the adjacent leading leg. In this investigation, we evaluate the hypothesis that a powered ankle–foot prosthesis, capable of providing human-like ankle work and power during stance, can decrease the metabolic cost of transport (COT) compared to a conventional passive-elastic prosthesis. To test the hypothesis, a powered prosthesis is built that comprises a unidirectional spring, configured in parallel with a force-controllable actuator with series elasticity. The prosthesis is shown to deliver the high mechanical power and net positive work observed in normal human walking. The rate of oxygen consumption and carbon dioxide production is measured as a determinant of metabolic rate on three unilateral transtibial amputees walking at self-selected speeds. We find that the powered prosthesis decreases the amputee’s metabolic COT on average by 14% compared to the conventional passive-elastic prostheses evaluated (Flex-Foot Ceterus<sup>®</sup> and Freedom Innovations Sierra), even though the powered system is over twofold heavier than the conventional devices. These results highlight the clinical importance of prosthetic interventions that closely mimic the mass distribution, kinetics, and kinematics of the missing limb.

**Index Terms**—Amputee gait, impedance control, parallel elasticity, powered prosthesis, series elasticity, walking metabolism .

## I. INTRODUCTION

**T**ODAY’S commercially available below-knee prostheses are completely passive during stance, and consequently, their mechanical properties remain fixed with walking speed and terrain. These prostheses typically comprise elastic bumper

springs or carbon composite leaf springs that store and release energy during the stance period, e.g., the Flex-Foot or the Seattle-Lite [1], [3].

Lower extremity amputees using these conventional prostheses experience many problems during locomotion. For example, transtibial amputees expend 20–30% more metabolic power to walk at the same speed as able-bodied individuals, and therefore, they prefer a 30–40% slower walking speed to travel the same distance [4], [5]. In addition, many clinical studies report that amputees exhibit an asymmetrical gait pattern [6]–[8]. For example, unilateral transtibial amputees generally have higher than normal hip extension, knee flexion, and ankle dorsiflexion on the unaffected side. On the affected side, such individuals have less than normal hip and knee flexion during stance. Additionally, there is a significant ankle power difference between the affected and unaffected sides during ankle-powered plantar flexion.

There are many differences between the mechanical behavior of conventional ankle–foot prostheses during the walking cycle and that of the human ankle–foot complex. Most notably, the human ankle performs net positive work and greater power over the stance period, especially at moderate to fast walking speeds [2], [9]–[12]. For example, at a self-selected walking speed (1.25 m/s), the human ankle provides  $\sim 0.10$  J/kg of net work [10] and  $\sim 3.5$  W/kg of peak positive power [2], [10]. Researchers hypothesize [13]–[15] that the inability of conventional passive prostheses to provide these human-like energetics is the main cause for the metabolic, speed and symmetry difficulties experienced by today’s transtibial amputees.

The objective of this investigation is to advance a powered ankle–foot prosthesis capable of mimicking human ankle dynamics in level-ground walking, and to assess whether the prosthesis has the capacity to improve amputee ambulation.

### A. Previous Work

Some recent research has focused on the development of quasi-passive ankle–foot prostheses. Researchers have built prostheses that use active damping or spring–clutch mechanisms to allow automatic ankle angle adjustment for distinct ground surfaces [1], [16]–[18], or to allow for an improved metabolic walking economy [19]. Since these devices do not include an actuator to actively plantar flex the ankle at terminal stance, no net work is performed throughout each walking step, as is the case with the human ankle [2], [9]–[12]. In 1998, Klute *et al.* [20] were the first to build a powered ankle–foot prosthesis capable of performing net positive work. Their device employed a pneumatic actuation strategy with off-board power. Recently, Versluis *et al.* [21] also designed a powered prosthesis with pneumatic actuation and offboard power. Other recent

Manuscript received March 28, 2008; revised August 26, 2008; accepted October 9, 2008. First published January 6, 2009; current version published February 4, 2009. This paper was recommended for publication by Associate Editor K. Yamane and Editor F. Park upon evaluation of the reviewers’ comments. This work was supported in part by the U.S. Department of Veteran’s Administration under Grant V650P-3945 as part of the Center for Restorative and Regenerative Medicine.

S. K. Au is with the Department of Mechanical Engineering, MIT Media Laboratory, Massachusetts Institute of Technology (MIT), Cambridge, MA 02139 USA (e-mail: kwau@mit.edu).

J. Weber is with the MIT Media Laboratory, Massachusetts Institute of Technology (MIT), Cambridge, MA 02139 USA, and also with Meka Robotics LLC, San Francisco, CA 94107 USA.

H. Herr is with the MIT Media Laboratory and the Harvard–MIT Division of Health Sciences and Technology, Massachusetts Institute of Technology (MIT), Cambridge, MA 02139 USA (e-mail: hherr@media.mit.edu).

Color versions of one or more of the figures in this paper are available online at <http://ieeexplore.ieee.org>.

Digital Object Identifier 10.1109/TRO.2008.2008747

work has focused on the design of energetically-autonomous powered systems [22]–[29].

### B. Engineering Challenges

According to [6], [30], and [31], two main engineering challenges hinder the development of a powered ankle-foot prosthesis.

- 1) *Mechanical design*: With current actuator technology, it is challenging to build an ankle-foot prosthesis that matches the size and weight of the human ankle, but still provides a sufficiently large instantaneous power output and torque to propel an amputee. The shank-ankle-foot complex of a 78 kg person weighs approximately 2 kg, while the peak power and torque at the ankle during walking can be as high as 350 W and 140 N·m, respectively [30], [31]. Current ankle-foot mechanisms for humanoid robots are not appropriate for this application, as they are either too heavy or not sufficiently powerful to meet the human-like specifications required for a prosthesis [32], [33].
- 2) *Control system design*: A powered prosthesis must be position- and impedance-controllable. Often robotic ankle controllers for humanoid robots follow preplanned kinematic trajectories during walking [32], [33], whereas the human ankle is believed to operate in impedance control mode during stance and position control mode during swing [9]–[11]. Furthermore, for ease of use, only local sensing on the prosthesis is preferable, which adds additional constraints on the control system design. Finally, it is unclear what kind of prosthetic control strategy is effective for the improvement of amputee ambulation.

### C. Objectives and Outline

A key objective of this research is to address both the mechanical and control system design challenges. We design and build a novel motorized prosthesis that exploits both series and parallel elasticity to fulfill the demanding human-like ankle specifications [30], [31]. To solve the control system problem, we design and evaluate a finite-state machine that can provide both impedance and position control for mimicking human ankle behavior during walking. We conduct a preliminary investigation to test the hypothesis that a powered ankle-foot prosthesis can decrease an amputee's metabolic cost of transport (COT), or the metabolic energy required to transport unit body weight unit distance, compared to a conventional passive-elastic device. Using measures of oxygen consumption and carbon dioxide production during level-ground walking at self-selected speeds, we estimate walking metabolic rates on three transtibial amputee participants using the powered prosthesis and conventional passive-elastic prostheses.

## II. DESIGN SPECIFICATIONS AND TARGET ANKLE STANCE BEHAVIORS FOR THE PROSTHESIS

In this section, we first review human ankle biomechanics in walking. Using these biomechanical descriptions, we then define the design specifications for the prosthesis.

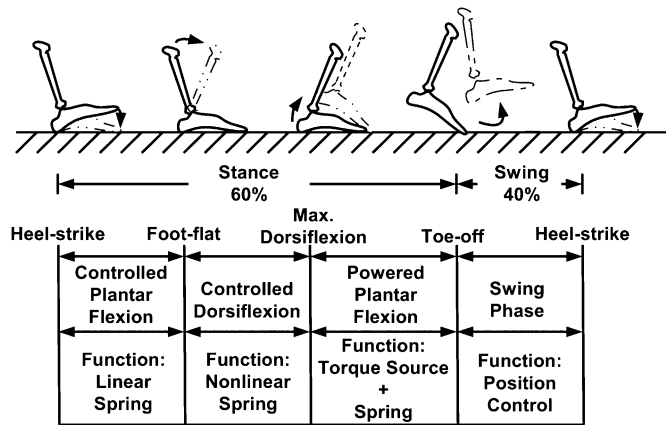


Fig. 1. Normal human ankle biomechanics for level-ground walking.

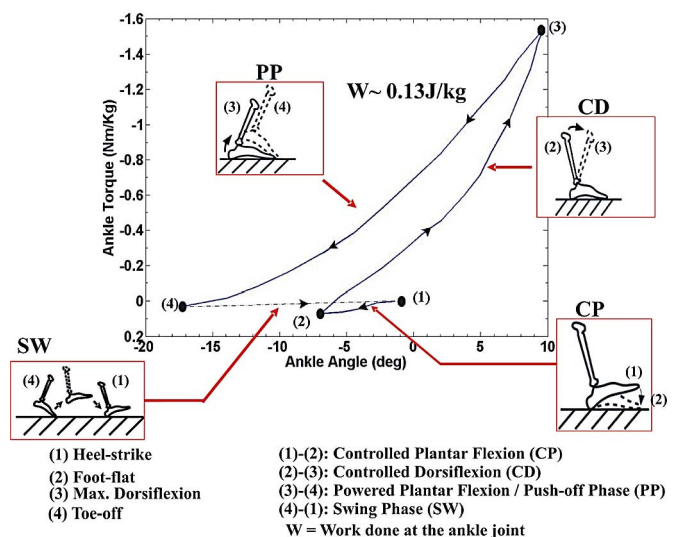


Fig. 2. Average ankle torque is plotted versus ankle angle for  $N = 10$  individuals with intact limbs walking at a moderate gait speed (1.25 m/s). Data are from [10], replotted in the manner of [31]. The solid line shows the ankle torque-angle behavior during stance while the dash line shows the ankle behavior during the SW. The points (1), (2), (3), and (4) represent the conditions of the foot at heel-strike, foot-flat, maximum dorsiflexion, and toe-off, respectively. The segments (1)–(2), (2)–(3), (3)–(4), and (4)–(1) represent the ankle torque-angle behaviors during CP, CD, PP, and SW phases of gait, respectively. Segments (1)–(2) and (2)–(3) reveal different spring behaviors of the human ankle during CP and CD, respectively. The area W enclosed by points (1), (2), (3), and (4) is the net work done at the joint per unit body mass during the stance period.

### A. Human Ankle Biomechanics in Walking

A level-ground walking cycle is typically defined as beginning with the heel strike of one foot and ending at the next heel strike of the same foot [35]. The main subdivisions of the gait cycle are the stance phase (60% gait cycle) and the swing phase (SW) (40% gait cycle) (Fig. 1). The SW represents the portion of the gait cycle when the foot is off the ground. The stance phase begins at heel-strike when the heel touches the ground and ends at toe-off when the same foot rises from the ground surface. From [9], [10], the stance phase of walking can be divided into three subphases: controlled plantar flexion (CP), controlled dorsiflexion (CD), and powered plantar flexion (PP). These phases of gait are described in Fig. 1. In addition, Fig. 2 shows the

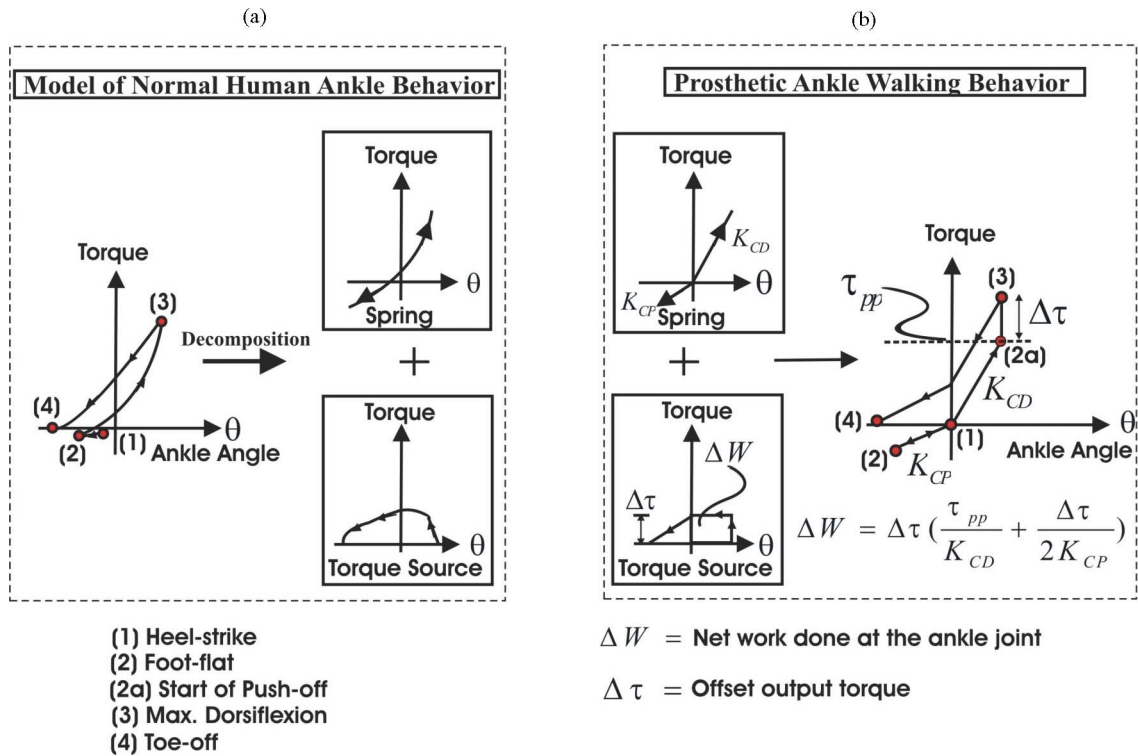


Fig. 3. Model of human ankle behavior.

average ankle torque–angle characteristics for  $N = 10$  individuals with intact limbs walking at a moderate speed (1.25 m/s). Detailed descriptions for each subphase are provided next.

- 1) *Controlled plantar flexion*: CP begins at heel-strike and ends at foot-flat. Simply speaking, CP describes the process by which the heel and forefoot initially make contact with the ground. In [9] and [10], researchers showed that ankle joint behavior during CP was consistent with a linear spring response with joint torque proportional to joint position. As shown in Fig. 2, segment (1)–(2) illustrates the linear spring behavior of the ankle.
- 2) *Controlled dorsiflexion*: CD begins at foot-flat and continues until the ankle reaches a state of maximum dorsiflexion. Ankle torque versus position during the CD period can often be described as a nonlinear spring where stiffness increases with increasing ankle position. The main function of the human ankle during CD is to store elastic energy to propel the body upward and forward during the PP phase [9]–[12]. Segment (2)–(3) in Fig. 2 reveals the nonlinear spring behavior of the human ankle joint during CD.
- 3) *Powered plantar flexion*: PP begins after CD and ends at the instant of toe-off. Because the work generated during PP is more than the negative work absorbed during the CP and CD phases for moderate to fast walking speeds [9]–[12], additional energy is supplied along with the spring energy stored during the CD phase to achieve the net ankle work and high plantar flexion power during late stance. Thus, during PP, the ankle can be modeled as a torque source in parallel to a CD spring. The area  $W$  enclosed by the points (1), (2a), (3), and (4) shows the amount of net work done at the ankle during the stance period.

- 4) *Swing phase*: SW begins at toe-off and ends at heel-strike. It represents the portion of the gait cycle when the foot is off the ground. During SW, the ankle can be modeled as a position source to achieve foot clearance as well as to reset the foot to a desired equilibrium position before the next heel strike.

In summary, for level-ground walking, the human ankle provides three main functions: 1) it behaves as a spring with variable stiffness from CP to CD; 2) it provides additional energy for push-off during PP; and 3) it behaves as a position source to control the foot orientation during SW.

## B. Target Stance Phase Behavior

Referring to Section I-B, the key question for the design and control of the prosthesis is to define a target walking behavior. For the SW, the desired ankle behavior is just to reposition the foot to a predefined equilibrium position. Although the equilibrium position of the ankle at heel strike should ideally be modulated between walking cycles based on walking speed and terrain, in this investigation we selected a fixed equilibrium position to simplify the control design.

For the stance phase control, instead of simply tracking human ankle kinematics, it is commonly believed that the prosthesis should mimic the human ankle’s “quasi-static stiffness,” i.e., the slope of the measured ankle torque–angle curve during stance [9], [10]. Mimicking the quasi-static stiffness curve of an intact ankle during walking (Fig. 2) is the main goal for the stance phase controller of this investigation.

As shown in Fig. 3(a), a typical quasi-static stiffness curve [from points (1)–(4)] can be decomposed into two main

components: spring and torque source. The first component comprises two springs fitted to the torque versus angle curve during the CP and CD phases [See Fig. 3(b)]. The second component comprises a torque source that represents the residual torque between the spring torque and the total human ankle torque. It is noted that the stiffness from points (1)–(2) is approximately equal to the stiffness in the first portion of CD. Thus, CP and the first portion of CD were modeled with a single spring as shown in Fig. 3(b).

For the ease of implementation, we simplified these two components (spring and torque sources) to obtain the target stance phase behavior for the prosthesis as depicted in Fig. 3(b). Specifically, we linearized the CD spring and torque source functions, and provided only the spring components during CP and CD since the torque source is negligible during these gait phases [see Fig. 3(a)]. Each component is described as follows.

- 1) The first component comprises a linear torsional spring with a stiffness that varies with the sign of the ankle angle. When the ankle angle is positive, the stiffness value is set to  $K_{CD}$ . When the ankle angle is negative, the stiffness value is set to  $K_{CP}$  [See Fig. 3(b)].
- 2) The second component comprises a constant offset torque  $\Delta\tau$  that provides the torque source during PP. This offset torque is applied in addition to the linear torsional spring  $K_{CD}$  during PP.  $\tau_{pp}$  determines the moment at which the offset torque is applied, indicated by point (4) in Fig. 3(b). The actual work done by the ankle joint due to the torque source  $\Delta W$  is

$$\Delta W = \Delta\tau \left( \frac{\tau_{pp}}{K_{CD}} + \frac{\Delta\tau}{2K_{CP}} \right). \quad (1)$$

It is noted here that conventional passive prostheses only provide the spring behavior but fail to supply the torque source function to further enhance propulsion during PP [3].

### C. Design Specifications

Using the aforesaid biomechanical descriptions and the results from [2], [9], [10], and [35], the design goals for the prosthesis are summarized as follows:

- 1) the prosthesis must have a mass distribution comparable to the missing human limb;
- 2) the system must deliver a human-like output power and torque during PP;
- 3) the system must be capable of changing its stiffness as dictated by the quasi-static stiffness of an intact ankle;
- 4) the system must be capable of controlling joint position during the SW;
- 5) the prosthesis must provide sufficient shock tolerance to prevent any damage to the mechanism at heel-strike.

It is important to note that the prosthesis and controller designs are not independent. Rather, they are integrated to ensure that the inherent prosthesis dynamics does not inhibit the controller's ability to specify desired dynamics. This

topic is discussed further in Section IV. In the remainder of this section, the target parameters for the design goals are outlined.

- 1) *Size and weight*: The target height for the prosthesis is specified, based on the nominal height of a conventional high profile below-knee prosthesis, which is about 18 cm from ground to pyramid dome [1], [3]. The desired prosthesis mass should be 2.5% of total body mass, equal to the percent mass of the missing biological limb at a point 18 cm from the ground surface [34].
- 2) *Range of joint rotation*: The proposed range of joint rotation for the prosthesis was based upon normal human ankle range of motion during walking [2], [35], [36]. The maximum plantar flexion angle ( $25^\circ$ ) occurs just as the foot is lifted off the ground at toe-off, while the maximum dorsiflexion angle ( $15^\circ$ ) occurs at terminal CD.
- 3) *Torque and speed*: According to [2], [9], [10], and [35], the measured peak velocity, torque, and power of the human ankle during the stance period of walking can be as high as 5 rad/s, 1.7 N·m/kg, and 3.5 W/kg, respectively. Both peak torque and power were normalized by body mass. Rather than simply satisfying these peak values, the torque-speed capability of the prosthesis was designed to cover the entire human ankle torque-speed curve of walking.
- 4) *Torque bandwidth*: The torque bandwidth requirement of the prosthesis was estimated based upon the power spectrum of the human ankle torque data during the stance period of walking. In this paper, the torque bandwidth was defined at that frequency range over which 70% of the total signal power was captured. Analyzing the normal human ankle data from [10], the torque bandwidth was found to be  $\sim 3.5$  Hz in which the ankle torque varies between 50 and 140 N·m. The goal was therefore to design a torque controller capable of outputting any torque level between 50 and 140 N·m at 3.5 Hz. This goal requires that the torque bandwidth of the open-loop system be significantly larger than 3.5 Hz, otherwise the inherent dynamics of the prosthesis may inhibit the controller's ability to specify desired dynamics.
- 5) *Net positive work*: The prosthesis should also be capable of generating net positive work during stance. The average net positive work done at the ankle joint per unit body mass for self-selected and fast walking speeds is  $\sim 0.10$  J/kg [2], [10] and  $\sim 0.26$  J/kg [9], respectively.
- 6) *Controlled dorsiflexion stiffness*: The prosthesis should output a human-like quasi-static stiffness during CD, or from point 2 to point 3 in Fig. 2. A target stiffness value was obtained by estimating the slope of the measured human ankle torque-angle curve from the zero torque-angle point to the torque at maximum dorsiflexion, or point 3 in Fig. 2. The average human stiffness per unit body mass at a self-selected walking speed is  $\sim 8$  N·m/rad·kg.

In this paper, we design an ankle-foot prosthesis for a nominal male subject, walking at a self-selected speed of 1.25 m/s, whose body mass, height, and foot length are 78 kg, 175 cm,

TABLE I  
 DESIGN SPECIFICATIONS FOR A NOMINAL MALE SUBJECT

Total Prosthetic Mass (kg)	2
Max. Allowable Dorsiflexion (deg)	15
Max. Allowable Plantarflexion (deg)	25
Peak Torque (Nm)	133
Peak Velocity (rad/s)	5
Peak Power (W)	274
Torque Bandwidth (Hz)	3.5
Net Work Done (J)	7.8
Controlled Dorsiflexion Stiffness (Nm/rad)	627

and 27 cm, respectively [37]. Table I lists the parameter values corresponding to the aforesaid design goals.

### III. MECHANICAL DESIGN

The basic architecture of our mechanical design is a physical spring, configured in parallel to a force-controllable actuator. Figs. 4 and 5 show the mechanical design and the schematics of the proposed powered prosthesis, respectively. As shown in Fig. 5, there are five mechanical elements in the system: a high power output d.c. motor, a ballscrew transmission, a series spring, a unidirectional parallel spring, and a carbon composite leaf-spring prosthetic foot. We combine the first three components to form a rotary series-elastic actuator (SEA). An SEA, previously developed for legged robots [38], [39], consists of a dc motor in series with a spring (or spring structure) via a mechanical transmission. By controlling the extent to which the series spring is compressed, the SEA can be used to control output force. In this investigation, we used a linear potentiometer to measure the deflection of the series spring, and the force applied to the load.

In this study, we used the SEA to modulate the joint stiffness as well as to provide the constant offset torque  $\Delta\tau$  defined in Fig. 6. The SEA also provided the stiffness value  $K_{CP}$  during CP and the stiffness value  $K_{CD1}$  during CD. During PP, the SEA also supplied both the stiffness value  $K_{CD1}$  and a constant, offset torque  $\Delta\tau$ .

Due to the demanding output torque and power requirements, we employed a physical spring, configured in parallel to the SEA, so that the load borne by the SEA could be greatly reduced. To avoid hindering ankle plantar flexion movements at terminal stance, the parallel spring was unidirectional, only providing an offset rotational stiffness value  $K_p^r$  when the ankle angle was greater than zero (see Fig. 6).

An elastic leaf spring foot was used to emulate the function of a human foot, providing shock absorption and energy storage during early stance, and energy return during late stance. A standard low profile prosthetic foot, called the Flex Foot LP Vari-Flex<sup>®</sup> was used in the prototype [1].

In the current design, a 150 W dc brushed motor from Maxon, Inc (RE-40) was used. For the drive train system, the motor was designed to drive a 3 mm pitch linear ballscrew via a timing-belt drive transmission with a 1.7:1 ratio. The translational movement of the ballscrew caused an angular rotation of the ankle joint via the series spring with a moment arm  $r = 0.0375$  m. Further details on the mechanical design and component selection can be found in [24].

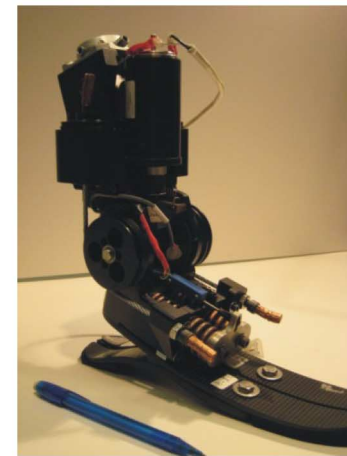
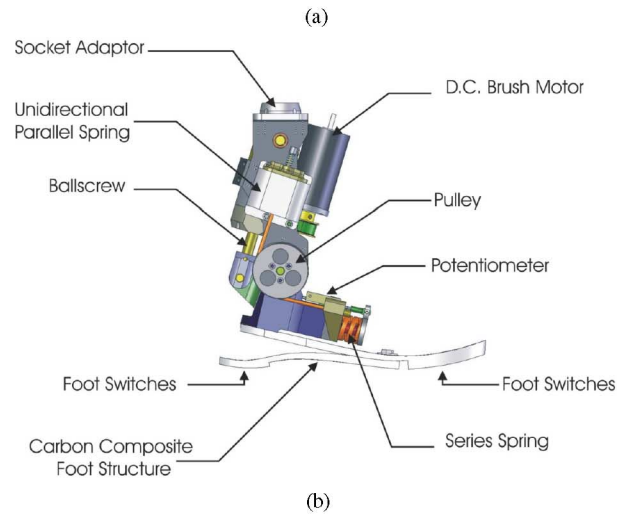
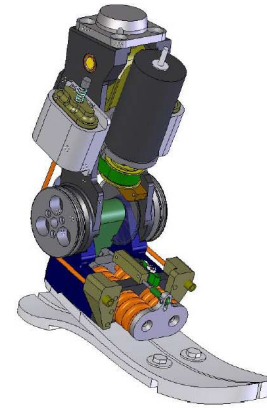


Fig. 4. Mechanical design of the prosthesis. (a) Front View. (b) Side View. (c) Physical Prototype.

### IV. SYSTEM MODEL

#### A. Linear Model

A linear model of the prosthetic device is shown in Fig. 7. The model is similar to the standard SEA model in [39], except for the addition of a parallel elastic component. Referring to Fig. 7(a), the motor is modeled as a torque source  $T_m$  with a

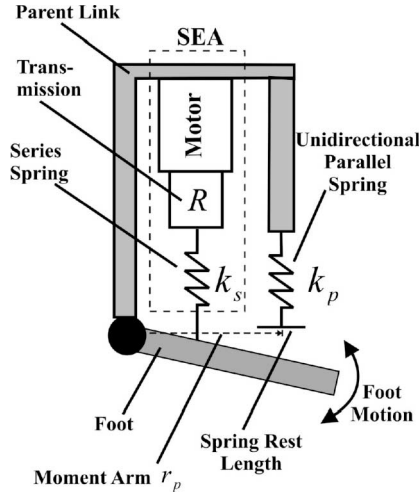


Fig. 5. Schematics of the powered ankle-foot prosthesis.

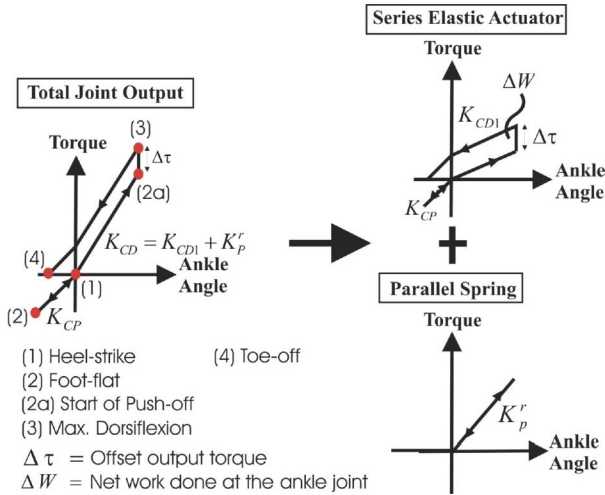


Fig. 6. Parallel and series elasticity. The parallel spring provides a biased, offset stiffness  $K_p^r$  when the ankle angle is larger than zero. The series spring combined with the motor and transmission, called an SEA [38], [39], was used to modulate joint stiffness and as a torque source for performing positive net work at the ankle joint.

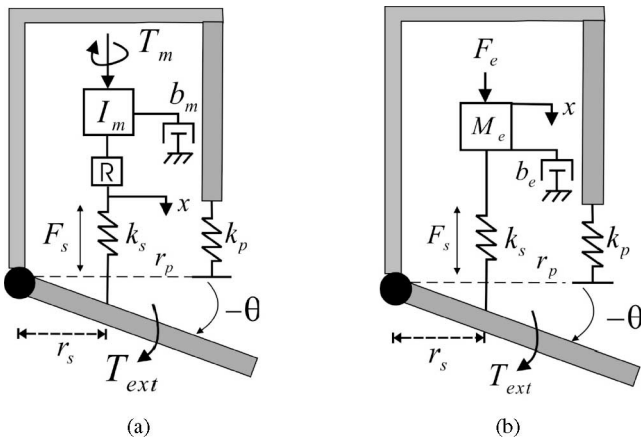


Fig. 7. Linear prosthesis models. (a) Rotary domain (b) Translational domain.

rotary internal inertia  $I_m$ , applying a force to a series spring of stiffness  $k_s$  through a transmission  $R$ . The damping term  $b_m$  represents brush and bearing friction acting on the motor, and  $k_p$  is the stiffness of a unidirectional parallel spring. The transmission has a ratio  $R$  that converts rotary motion of the motor into linear compression of the series spring. The series spring moment arm is  $r_s$ , and the parallel spring moment arm is  $r_p$ . Further,  $T_{ext}$  and  $\theta$  are the external joint torque and angular displacement, respectively. In the model, we assume the foot is a rigid body of negligible mass, as foot mass is relatively small compared to the effective motor inertia. This model also ignores amplifier dynamics, nonlinear friction, and internal resonances.

For simplicity, we convert this rotary model into the translational domain [see Fig. 7(b)]. Effective mass  $M_e$ , damping  $b_e$ , and linear motor force  $F_e$  are defined as follows:  $M_e = I_m R^2$ ,  $F_e = T_m R$ , and  $b_e = b_m R$ . The equation of motion then becomes

$$M_e \ddot{x} + b_e \dot{x} = F_e - F_s \quad (2)$$

$$F_s = k_s (x - r_s \theta) \quad (3)$$

where  $F_s$  is the force applied by the series spring. The total external joint torque is

$$T_{ext} = \begin{cases} r_s F_s, & \theta < 0 \\ r_s F_s + r_p k_p \theta, & \theta \geq 0. \end{cases} \quad (4)$$

Equations (2) and (3) are the standard dynamic equations for an SEA [39]. Equation (4) reveals that with the parallel spring, less series spring force  $F_s$  is required for a given total joint torque.

### B. Force Bandwidth

When designing a controller, one needs to guarantee that the actuator system does not saturate within the desired operating range of torque and speed. A critical actuator performance metric is the open-loop force bandwidth (OFB). OFB is defined as the frequency response of the system output force due to the maximum input motor force  $F_{sat}$ . The higher the OFB is for the system, the better the prosthetic controller can capture the nominal behavior of the human ankle in walking without saturating the motor. Due to motor saturation, the OFB generally increases as actuator force requirements decrease. The lower the required actuator force, the higher the frequency capability of sinusoidal tracking. Thus, parallel elasticity increases the OFB, since force levels borne by the actuator are effectively lowered. Although ankle shock tolerance is improved when a spring is placed in series with the motor and transmission, the OFB is reduced as a consequence. Thus, when designing a motorized ankle-foot prosthesis, series spring stiffness has to be carefully selected so as to provide adequate actuator shock tolerance and OFB. Thus, when designing the ankle-foot prosthesis, we selected a series spring stiffness,  $k_s$ , so as to provide a sufficient actuator shock tolerance and OFB (see Table I for bandwidth specification) at the lowered peak actuator force enabled by parallel elasticity. Because of parallel elasticity, series spring stiffness could be decreased while still achieving adequate OFB. Lower series stiffness was beneficial since shock tolerance was improved.

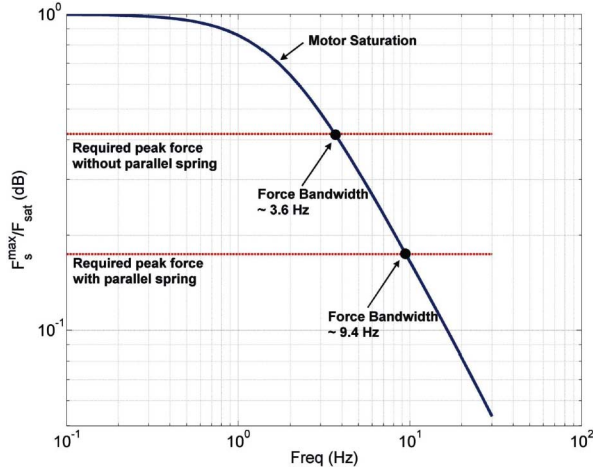


Fig. 8. Simulation result showing the open-loop force bandwidth values due to motor saturation at each actuator force level. A relatively stiff series spring was selected to obtain an open-loop force bandwidth equal to 9.4 Hz, a value that is significantly larger than the bandwidth specification of 3.5 Hz in Table I.

TABLE II  
MODEL PARAMETERS

Parameters	$F_{sat}$	$V_{sat}$	$M_e$	$B_e$
Values	7654N	0.23m/s	170kg	8250Ns/m

To study the OFB, we set the ankle angle,  $\theta$ , equal to zero in Fig. 7(b), making the equation of motion (2) for this model equivalent to a standard second-order differential equation for a spring–mass–damper system. With the spring force,  $F_s$ , considered as the system output, the transfer function that describes the OFB due to the maximum input motor force  $F_{sat}$  is

$$\frac{F_s^{max}}{F_{sat}} = \frac{k_s}{M_e s^2 + (B_e + \frac{F_{sat}}{V_{sat}})s + k_s} \quad (5)$$

where  $F_s^{max}$  and  $V_{sat}$  are the maximum output spring force and linear velocity, respectively. We set  $F_{sat} = RT_{motor}^{max}$  and  $V_{sat} = \frac{\omega^{max}}{R}$ . As can be seen in (5), the OFB is independent of the control system, depending only on the intrinsic system behaviors determined by the motor, transmission ratio, and spring constants. In our design, the total spring constant for the series springs was set to 1200 kN/m.

The simulation results for the OFB are shown in Fig. 8 and the corresponding parameter values used in the model are listed in Table II. The estimated OFB of the system with and without parallel elasticity was 9.4 Hz (at 50 N·m) and 3.8 Hz (at 120 N·m), respectively. In practice, it is wise to design a system with an OFB that is at least twofold larger than the required bandwidth, as there are many factors that can substantially reduce the force bandwidth, such as unmodeled friction [39]. With the parallel spring set equal to 373 kN·m/rad and the linear series spring stiffness equal to 1200 kN/m, the estimated OFB from the model was 9.4 Hz, nearly threefold larger than the required bandwidth of 3.5 Hz from Table I. Thus, the ankle–foot prosthetic design had an OFB that was sufficiently large to ensure that the motor would not saturate within the desired operating range of torque and speed.

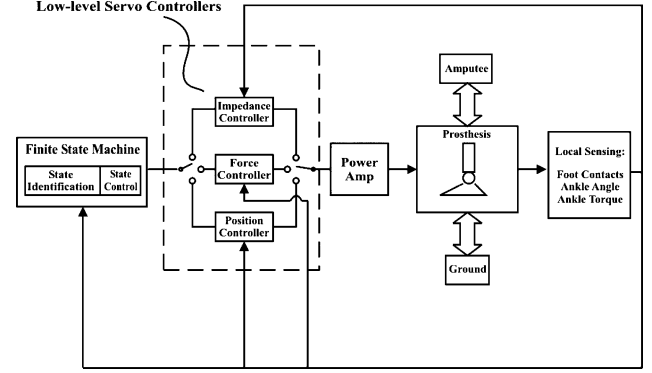


Fig. 9. Overall control architecture of the prosthesis.

## V. CONTROL SYSTEM

### A. Overall Architecture

Referring to Section II-B, the goal of the control system was to allow the prosthesis to track the target stance phase behavior shown in Fig. 3(b). To this end, the prosthesis had three types of low-level servo controllers: 1) a high performance torque controller to provide the ankle push-off during powered plantar flexion; 2) an impedance controller to modulate joint stiffness during the entire stance phase; and 3) a position controller to control foot position during the SW.

Furthermore, it was necessary to have a high-level control system to manage the transitions among the low-level servo controllers so as to provide proper prosthetic functions for a given condition. The overall architecture of the control system is shown in Fig. 9. The control system comprised a set of low-level servo controllers and a finite-state machine, widely used in the high-level control of A/K prostheses [41], [42]. The finite-state machine had two parts: a state identification and a state control. The former was used to identify the current state of the prosthesis while the latter was used to execute the predefined control procedure for a given state. In the following sections, we first discuss the development of the low-level servo controllers, followed by the design of the finite-state machine.

### B. Low-Level Servo Controllers

Throughout this section, we assume that the parallel spring does not inhibit the controllers' ability to specify desired dynamics, at least within the operating range of torque level and bandwidth.

1) *Torque Controller*: A torque controller was designed to provide the offset torque and facilitate the stiffness modulation. The primary design concern was to satisfy the bandwidth constraint specified in Table I. The design consisted of 1) an inner force/torque control loop and 2) a feedforward friction compensation term [see Fig. 10(a)]. The basic concept of the inner force/torque control loop was to use the force feedback, estimated from the series spring deflection, to control the output joint torque of the SEA [39]. The torque/force controller  $D(s)$  was essentially implemented based on a PD control law



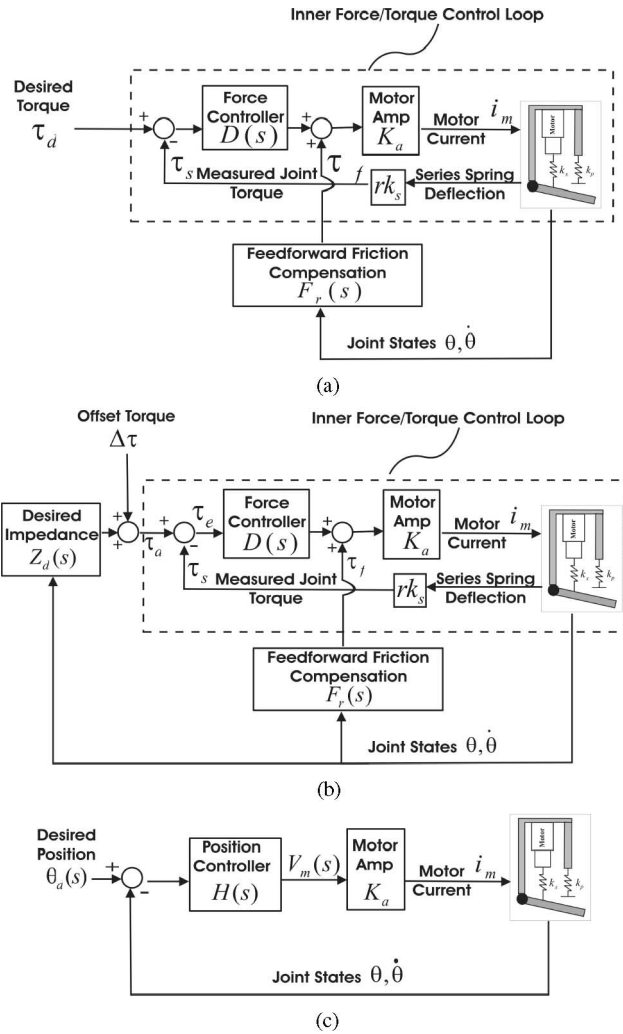


Fig. 10. Block diagrams for the low-level servo controllers. (a) Torque controller. (b) Impedance controller. (c) Position controller.

(in S-domain)

$$D(s) = \frac{V_m(s)}{\tau_e(s)} = K_F + sB_F \frac{p}{s+p} \quad (6)$$

where  $\tau_e$  and  $V_m$  are the output torque error and input voltage to the motor amplifier, respectively. Furthermore,  $K_F$  and  $B_F$  are the proportional gain and damping of the control law, respectively. A simple dominant pole filter  $\frac{p}{s+p}$  was incorporated into the controller because often the measured force signal was very noisy and had to be filtered before a derivative was taken. The pole  $p$  of the controller was set to accomplish a cutoff frequency of 30 Hz, a value that is sufficiently larger than the required torque bandwidth listed in Table I.

Although increasing the gain  $K_F$  can shadow the intrinsic impedance (e.g., friction or inertia) in the mechanism, it may trigger instability when the system couples to certain environments at high gain [46], [47]. One way to augment the torque controller without violating the stability criteria is to use a model-based friction compensation term  $F_f(s)$ . A standard feedforward friction compensation term was applied into the

torque controller and defined as

$$\tau_f = f_c(\tau)\text{sgn}(\dot{\theta}) + b_c\dot{\theta} \quad (7)$$

where  $f_c$  and  $b_c$  are the Coulombic force constant and damping coefficient, respectively [48]. All these parameters were identified using experimental data.

To obtain the friction parameters, we set the ankle angle equal to zero [see Fig. 7(b)]. The friction in the ankle joint was negligible as compared to the friction in the transmission. We applied a known ramping input motor force to the system and measured the series spring compression. The Coulombic friction force was obtained based on the difference between the known input motor force and the series spring force. We then applied different frequencies of sinusoidal motor force to the system to obtain the frequency of the system, and then fitted the data to a spring–mass–damper model, without considering the motor saturation, to obtain the damping coefficient. The Coulombic force constant and damping coefficient used in the controller were 0.03 V (23 N) and 1.64 V·s/rad (1240 N·s/rad), respectively.

2) *Impedance Controller*: An impedance controller was designed to modulate the output impedance of the SEA, especially the joint stiffness. As shown in Fig. 10(b), we introduced an outer impedance control loop [ $Z_d(s)$ ] onto the proposed force controller to modulate the output impedance. The outer impedance control loop was based on the structure of the “Simple Impedance Control,” proposed by Hogan [43]. The key idea was to use the motion feedback from the ankle joint ( $\theta$ ) to increase the output joint impedance. The outer impedance controller is defined as

$$Z_d(s) = \frac{\tau_d(s)}{s\theta(s)} = \left( B_d + \frac{K_d}{s} \right) \quad (8)$$

where  $\tau_d$ ,  $K_d$ , and  $B_d$  are the desired SEA output joint torque, stiffness, and damping, respectively. Taking into consideration the parallel elasticity, the total joint impedance  $Z_{\text{total}}(s)$  is

$$Z_{\text{total}} = \begin{cases} \left( B_d + \frac{K_d}{s} \right), & \theta \leq 0 \\ \left( B_d + \frac{K_d + K_p^r}{s} \right), & \theta > 0. \end{cases} \quad (9)$$

Due to the intrinsic impedance (e.g., friction and inertia), the actual output impedance consisted of the desired output impedance due to the controller plus that due to the mechanism. For this reason, the aforementioned torque controller was incorporated into the impedance controller to reduce the effects of the intrinsic impedance.

3) *Position Controller*: A standard PD-controller  $H(s)$  was proposed to control the equilibrium position  $\theta_1$  of the foot during swing. Thus, the input voltage  $V_m(s)$  to the motor amplifier is  $V_m(s) = K_1(\theta_1 - \theta) + K_2\dot{\theta}$ , where  $K_1$  and  $K_2$  are the proportional and derivative terms of the controllers.

### C. Finite-State Controller

A finite-state controller for level-ground walking was implemented to replicate the target ankle behavior (Fig. 11). The

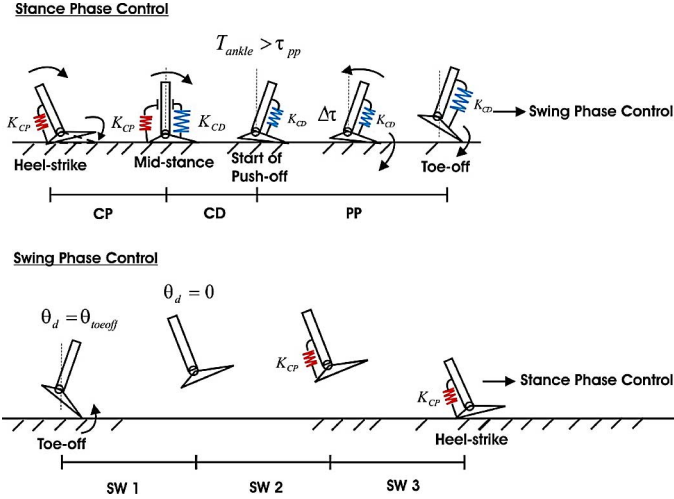


Fig. 11. Finite-state control for a typical gait cycle.

controller had two parts: stance and SW controls. Each part of the controller had three states.

1) *Stance Phase Control*: Three states (CP, CD, and PP) were designed for stance phase control. The stance phase control for a typical gait cycle is graphically depicted in Fig. 11. Descriptions for each state are as follows.

- CP begins at heel-strike and ends at midstance. During CP, the prosthesis outputs a joint stiffness,<sup>1</sup>  $K_{CP}$  to prevent foot slap and to provide shock absorption during heel-strike.
- CD begins at midstance and ends right before PP or toe-off, depending on the measured total ankle torque  $T_{ankle}$ . During CD, the prosthesis outputs a joint stiffness,  $K_{CD}$  to allow a smooth rotation of the body, where  $K_{CD} = K_p^r + K_{CD1}$ .
- PP begins only if the measured total ankle torque  $T_{ankle}$  is larger than the predefined torque threshold  $\tau_{pp}$ , i.e.,  $T_{ankle} > \tau_{pp}$ . Otherwise, it remains in state CD until the foot is off the ground. During PP, the prosthesis outputs a constant offset torque,  $\Delta\tau$  superimposing the joint stiffness,  $K_{CD}$  as an active push-off.

$K_{CP}$ ,  $K_{CD}$ ,  $\tau_{pp}$ , and  $\Delta\tau$  were the main parameters affecting the ankle performance during the stance phase control. In particular, the offset torque was directly related to the amount of net work done at the ankle joint. These parameter values were chosen based on the user's walking preference during experiments.

2) *Sw Control*: Another three states (SW1, SW2, and SW3) were designed for the SW control (see Fig. 11). Descriptions for each state are as follows.

- [a] SW1 begins at toe-off and ends in a given time period,  $t_H$ . During SW1, the prosthesis servos the foot to a predefined foot position,  $\theta_{toeoff}$  for foot clearance.
- SW2 begins right after SW1 and finishes when the ankle angle reaches zero. During SW2, the prosthesis servos the

<sup>1</sup>The conversion of the joint stiffness between translational and rotary domains is  $K = r^2 k$ , where  $k$  and  $r$  are the joint stiffness in translational domain and the moment arm, respectively. For example,  $K_{CP} = r^2 k_{CP}$ .

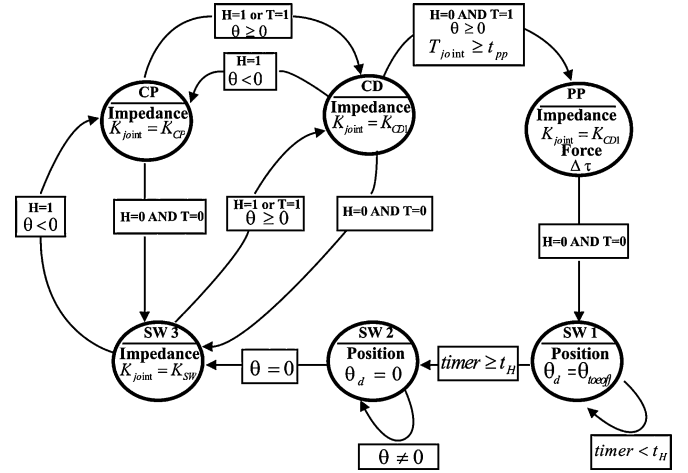


Fig. 12. Finite-state controller for level-ground walking.

ankle back to the default equilibrium position  $\theta_d = 0$  to prepare for the next heel-strike.

- SW3 begins right after SW2 and ends at the next heel-strike. During SW3, the controller resets the system to impedance control mode and outputs a joint stiffness,  $K_{CP}$ .

It was important to have state SW3 in the SW control to ensure the control system operated in impedance mode before heel-strike. Because of the rapid impact of heel-strike, there was not enough time for the control system to switch from position control mode at the moment of heel-strike without causing an appreciable state switching delay. The time period  $t_H$  and predefined foot position  $\theta_{toeoff}$  were all tuned experimentally.

3) *Sensing for State Transitions*: During state transition and identification, the system mainly relied on four variables.

- Heel contact(H). H=1 indicates that the heel is on the ground, and vice versa.
- Toe contact(T). T=1 indicates that the toe is on the ground, and vice versa.
- Ankle angle ( $\theta$ ).
- Total ankle torque ( $T_{ankle}$ ).

All triggering information was obtained using local sensing; including foot switches to measure heel/toe contact, ankle joint encoder to measure ankle angle, and a linear spring potentiometer to measure joint torque. The hardware implementation for these local sensors is discussed in the next section. The finite-state control diagram indicating all triggering conditions is shown in Fig. 12.

## VI. SENSORS AND COMPUTING PLATFORM

We installed a 5 k $\Omega$  linear potentiometer across the series springs to measure their displacement. We also mounted a 500-line quadrature encoder (US Digital, Inc.) in between the parent link mounting plate and child link mounting plate to measure the joint angle of the prosthetic ankle. Six capacitive force transducers were placed on the bottom of the foot: two sensors beneath the heel and four beneath the forefoot region. Using cabling, the prosthesis was connected to a multifunctional

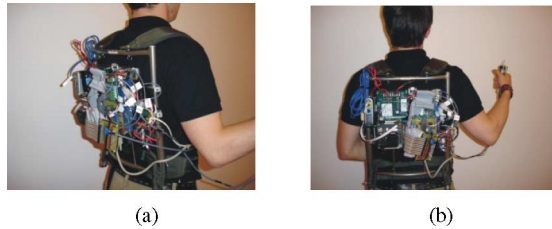


Fig. 13. Mobile computing platform was designed to provide the capability of testing the system outside the laboratory. (a) Lateral View. (b) Posterior View.

input/output (I/O) board from Sensory Company, Inc. (Model 526) that was interfaced with a PC104 Pentium III CPU (MSMP3XEG, from Advanced Digital Logic, Inc). The system ran the MMATLAB kernel for xPC target application [49]. The target PC (PC104) communicated with a host computer via Ethernet. The host computer sent control commands and obtained sensory data from the target PC104. We powered the dc motor with a motor amplifier (Accelnet Panel ACP-090-36,  $V = 48$  V,  $I_{pk} = 36$  A) from Copley Controls Corporation.

Finally, a mobile computing platform was developed that allowed us to conduct untethered walking experiments outside the laboratory. As shown in Fig. 13, the mobile platform was mounted on an external frame backpack. Most of the electronic components were mounted on the platform, including a PC104, a power supply, I/O Cards, and a motor amplifier.

## VII. CLINICAL EVALUATION

A common approach to evaluate the performance of a leg prosthesis is to measure the amputee's rate of oxygen consumption and carbon dioxide production in walking, as these measures correlate with metabolic rate [4], [5]. In this investigation, we took these measures on three unilateral transtibial amputees walking at self-selected speeds. Initial walking experiments were performed at Massachusetts Institute of Technology (MIT) on the Johnson Indoor Track. The experiments were approved by MIT's Committee on the Use of Humans as Experimental Subjects. The participants were volunteers and were permitted to withdraw from the study at any time and for any reason. Before taking part in the study, each participant read and signed a statement acknowledging informed consent.

### A. Experimental Participants

Three unilateral transtibial amputees participated in the study. Amputee participants were experienced at prosthesis ambulation, could ambulate at least at a K3 level (i.e., the patient has the ability or potential for ambulation with variable cadence) and had no other musculoskeletal problems or any known cardiovascular, pulmonary, or neurological disorders. The three participants (all male) were 40–57 years old, 173–176 cm in height, and weighed 71–86 kg. Patient characteristics are summarized in Table III.

### B. Experimental Protocol

The study comprised two sessions: Basic Clinical Gait Study and Metabolic Cost Study. The first session took place in the Biomechanics Laboratory within the MIT Media Laboratory. Before beginning the first session, each participant was fitted with the powered prosthesis by a professional prosthetist. Each participant was then asked to walk along a 30-foot-long walkway at his self-selected speed. The prosthesis was first programmed with a virtual spring response with stiffness values ( $K_{CP}$ ,  $K_{CD}$ ) from normalized biological data<sup>2</sup> [10]. The prosthetist then further refined the alignment using standard prosthetic alignment procedures. After this alignment procedure, each participant was given the option of making adjustments to the desired stiffness values ( $K_{CP}$ ,  $K_{CD}$ ) by communicating to a separate operator. The prosthesis was then programmed to output the active torque source response superimposed on the stiffness response during PP [See Fig. 3(b)]. The parameter values for the torque source response, including the predefined torque threshold ( $\tau_{pp}$ ) and the offset torque ( $\Delta\tau$ ), were initially set based on normalized biological values. Each participant was then given the option of making adjustments to the torque source parameters ( $\tau_{pp}$ ,  $\Delta\tau$ ) until they achieved the most favorable prosthetic ankle response. After these parameter adjustments, each participant's self-selected walking speed was measured. At that walking speed, ankle angle and torque were measured using the onboard ankle sensors.

In the second session, the rates of oxygen consumption and carbon dioxide production were measured to estimate metabolic cost. Before the second session began, each participant had approximately 5 h of acclimatization on the powered prosthesis. The metabolic measures were taken while each participant walked at a self-selected speed using: 1) their conventional prosthesis; 2) the powered prosthesis with a virtual spring response; and 3) the powered prosthesis with a nonconservative, motive power output. Before each trial, a participant was given 10 min to walk with each prosthesis to acclimatize to the new hardware. Walking speed was controlled by having the participant follow a modified golf cart moving at a desired speed. The self-selected walking speed with the powered prosthesis obtained in condition 3 was used for all three conditions. As with the first experimental session, sensory data (e.g., joint torque and angle) from the prosthesis was captured during the experiment. Each participant was advised not to have intense or prolonged exercise for 24 h prior to the experimental session. Furthermore, each participant was instructed to stay hydrated and not to have caffeine or a heavy meal 3 h before the experimental session.

### C. Metabolic Cost of Transport

The metabolic COT has been widely used to evaluate the performance of prosthetic leg interventions [4], [5]. The COT,  $C_m$ , is a dimensionless quantity defined as the metabolic energy

<sup>2</sup>In [10], ankle torque was normalized by body mass, and plotted versus ankle position. Thus, to get actual ankle stiffness values, we first multiplied the normalized biological data by the study participant's body mass before taking the slope (stiffness) of the ankle torque-position data.

TABLE III  
 AMPUTEE PARTICIPANT CHARACTERISTICS AND SELF-SELECTED WALKING SPEED

Subject #	Gender	Age (yrs)	Height (cm)	Weight (kg)	Speed (m/s)	Conventional Prosthesis	Cause of Amputation
1	M	45	176	86	1.38	Flex-Foot	Trauma
2	M	57	174	71	1.45	Flex-Foot	Trauma
3	M	40	173	75	1.68	Freedom	Trauma

required to transport unit body weight unit distance, or

$$C_m = \frac{\text{Metabolic Energy}}{\text{Total Weight} \times \text{Distance Traveled}}. \quad (10)$$

The total weight in (10) is the weight of the participant plus the weight of any prosthetic component worn by the participant. The distance traveled was obtained by multiplying the walking speed by the time period  $T$  over which the total energy was calculated.

The net metabolic energy  $E_m$  is normally obtained by integrating the net metabolic energy expenditure rate  $\dot{E}_m$  for a given time period  $T$

$$E_m = \int_0^T \dot{E}_m dt. \quad (11)$$

Equation (10) then becomes

$$C_m = \frac{E_m}{Mg\nu T} \quad (12)$$

where  $M$ ,  $g$ , and  $\nu$  are the mass of the participant plus the prosthetic system, gravity constant, and the average forward speed, respectively. The net metabolic rate  $\dot{E}_m$  was obtained by subtracting the resting metabolic rate from the measured metabolic rate of walking.

#### D. Measurement of COT

The energy cost was estimated from  $O_2$  consumption and  $CO_2$  production measured with a portable K4 telemetric system [50]. The K4 system included a portable unit worn by the subject and a base station where the data were recorded. The portable unit weighed 1.5 kg and consisted of a silicon mask containing a flow-rate turbine that was fixed to the subject's face. A processing unit containing the  $O_2$  and  $CO_2$  analyzers was placed on the subject's chest, and a transmitter/battery pack was placed in the backpack.

During each trial, the participant walked on the track for 5 min while metabolic data were recorded. Rest measurements were taken while the participant was seated for 5 min before and after each walking trial. The resting  $\dot{V}_{O_2}$  and  $\dot{V}_{CO_2}$  values were subtracted from the walking trial data to give the net values of  $\dot{V}_{O_2}$  and  $\dot{V}_{CO_2}$  (in milliliters per second). These values were then used to estimate the net metabolic rate  $\dot{E}_m$  for each walking trial using the formula from [51]

$$\dot{E}_m = 16.48\dot{V}_{O_2} + 4.48\dot{V}_{CO_2}. \quad (13)$$

The cumulative metabolic energy consumed at each trial time was plotted versus time. When the plotted data showed a line of constant slope, steady state energy consumption was assumed (as an example, see Fig. 18). We used the steady state portion of the cumulative energy versus time curve to compute the metabolic cost of transport for each walking trial.

 TABLE IV  
 SYSTEM MASS

Component Mass (kg)	Participant		
	1	2	3
Body	86	71	78
Battery	1.2	1.2	1.2
Mobile Computing Platform	2.9	2.9	2.9
Powered Prosthesis	2.9	2.9	2.9
Prosthetic System(Conventional)	1.8	2.2	1.9
Prosthetic System(Powered or Virtual Spring)	2.9	4.3	3.7
Total Mass (Conventional)	92.2	77.6	84.3
Total Mass (Powered or Virtual Spring)	94.5	80.9	87.3

The total weight in (10) was computed based on the following formula: Total Weight + Body Weight + Battery Weight + Weight of the Computing Platform + Weight of the K4 system + Prosthetic System Weight. The prosthetic system weight included the weight of the ankle-foot prosthesis and other components that were used to fit that prosthesis onto the participant, such as the socket adaptor and prosthetic socket. The body weight was the weight of a participant without wearing any prosthesis. The battery weight was set to be zero when calculating the Total Weight of each participant for condition (1). The numerical values of component mass for all the participants and experimental conditions are listed in Table IV.

## VIII. RESULTS

In this section, we present the results from the clinical gait evaluation of the powered and conventional prostheses. Bench test evaluations of the proposed ankle controllers can be found in [28].

#### A. Basic Clinical Gait Study

During the experiments, it was discovered that the proposed finite-state machine performed robustly and was capable of mimicking the target stance phase behavior. All amputee participants and the prosthetist were satisfied with the performance of the prosthesis. In general, it took less than 20 min for each amputee participant to adapt to the powered prosthesis. The prosthetist reported that with the powered device each participant moved with a more natural gait than with their conventional passive-elastic prosthesis. The preferred system parameters ( $K_{CP}$ ,  $K_{CD}$ ,  $\tau_{pp}$ ,  $\Delta\tau$ ) for each participant were recorded (See Table V). These particular parameters were used for the metabolic cost study.

1) *Virtual Spring Response*: Fig. 14 shows real-time data for two gait cycles of a walking experiment. As was proposed in Fig. 12, the system went through the state sequence 0-1-2-0 for each gait cycle under the virtual spring condition [see Fig. 14(d)]. The corresponding ankle torque-angle behavior of one gait cycle is shown in Fig. 15. This experimental result

TABLE V  
PARTICIPANT'S PREFERRED SYSTEM PARAMETERS

System Parameters	Participant		
	1	2	3
$K_{CP}$ (Nm/deg)	6.6	5.4	3.2
$K_{CD}$ (Nm/deg)	12.0	9.3	12.0
$\tau_{PP}$ (Nm)	80	45	80
$\Delta\tau$ (Nm)	90	90	65
$\Delta W$ (J)	21.0	20.7	19.1

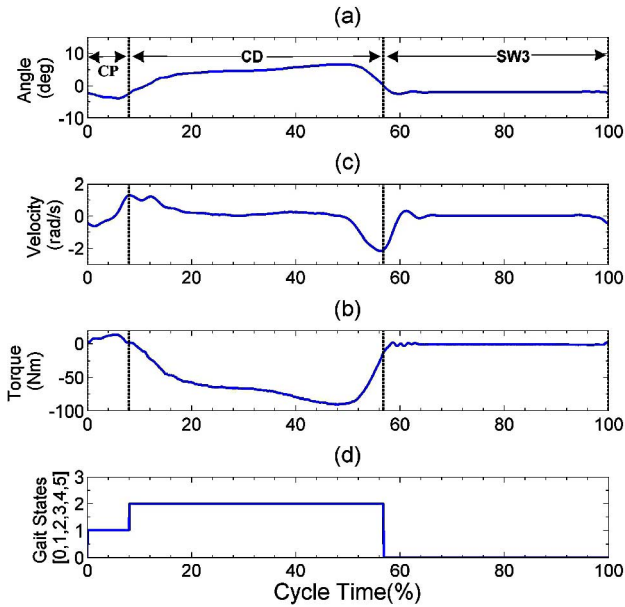


Fig. 14. Measured ankle angle, velocity, torque, and the gait states of a walking trial in which the prosthesis behaved as a virtual spring (participant 1). The gait states are defined as following: CP = 1, CD = 2, PP = 3, SW1 = 4, SW2 = 5, and SW3 = 0.

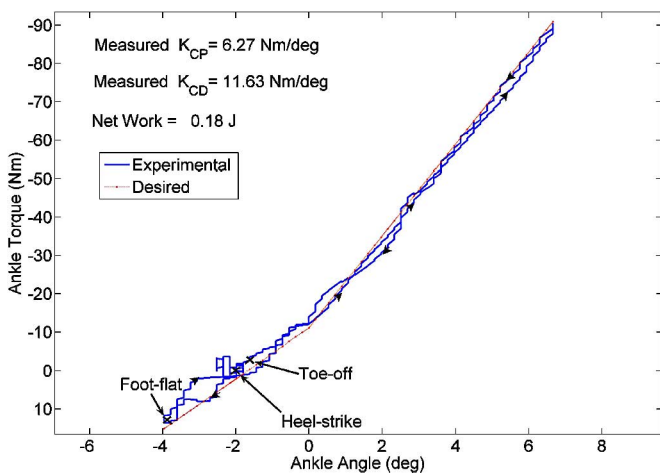


Fig. 15. Experimental ankle torque-angle plot for the powered prosthesis across a single gait cycle using the virtual spring controller (participant 1).

demonstrates the system's capacity to track the desired stiffness during CP and CD. As can be seen, the actual stiffness curve is slightly off from the desired curve because, in the physical system, the engagement position of the unidirectional parallel spring was not exactly equal to zero degree. This error caused the motor system to preload the spring at the equilibrium position.

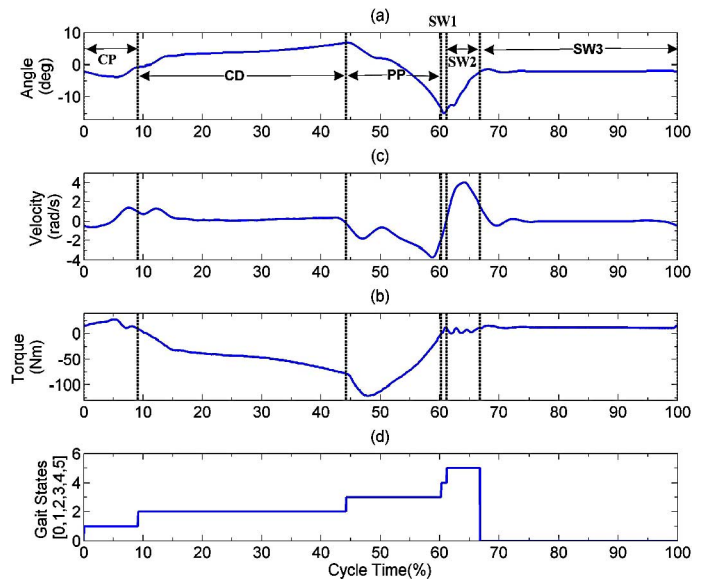


Fig. 16. Measured ankle angle, velocity, torque, and the gait states of a walking trial in which the prosthesis performed positive net work (participant 1). The gait states are defined as following: CP = 1, CD = 2, PP = 3, SW1 = 4, SW2 = 5, and SW3 = 0.

It was expected that the measured stiffness curve would show fluctuations at heel strike because the control system was not designed to satisfy such demanding bandwidth requirements. This justified the use of an SEA as the force-controllable actuator because with series elasticity, even if the movement of the prosthesis was much faster than the bandwidth of the control system, the prosthesis could still behave as a spring to prevent excessive impact loads on the transmission [39]. Additionally, the amputee user could always perceive a "springy feel" even though his foot hits the ground with great speed and force. In such a situation, the actual spring stiffness perceived by the participant was a value in between the desired stiffness  $K_{CP}$  and the stiffness of the series spring  $K_s$ .

2) *Active Mechanical Power*: Fig. 16 shows real-time data for two gait cycles of a walking experiment in which the powered prosthesis provides positive net work during stance. As is shown in Fig. 11, the system went through a longer state sequence 0-1-2-3-4-5-0 than that under the virtual spring condition [see Fig. 16(d)]. It is noted here that a rapid change in ankle velocity occurred from 60% to 70% of the gait cycle. Such a high dorsiflexion speed is critical immediately following toe-off to provide the amputee participant adequate foot clearance with the ground. This prosthetic movement occurred due to the position controller that set the ankle position back to zero degree in preparation for the next heel strike.

Fig. 17 shows the ankle torque-angle behavior of the prosthesis over five gait cycles. The experimental result demonstrates the system's capacity to track the desired stiffness during CP and CD. Furthermore, as was designed, a constant offset torque  $\Delta\tau$  was applied to the amputee participant when the ankle torque was larger than the triggering threshold  $\tau_{PP}$  (see the parameter values for participant 1 in Table V).

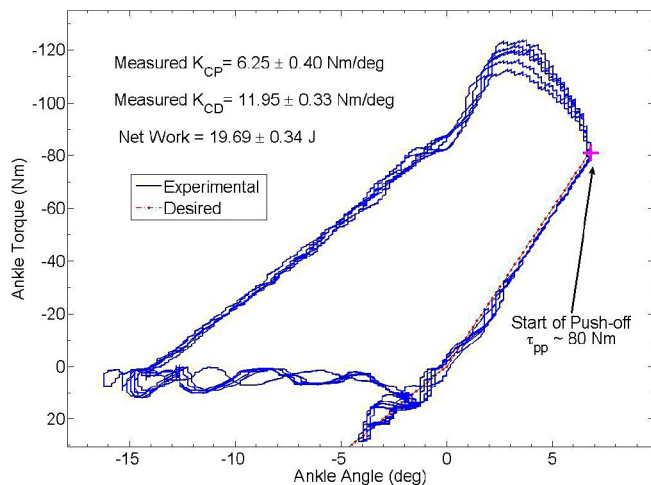


Fig. 17. Experimental ankle torque–angle plot for the powered prosthesis over five gait cycles with positive net work (participant 1). The red cross indicates the time at which the prosthesis begins actively plantar flexing.

It is noted that the measured ankle torque–angle curve flattens around the peak torque region, and consequently, there is a discrepancy between the estimated net work (21.0 J) and the measured mean net work (19.7 J). Here, the estimated net work was computed using (1), while the measured net work was obtained numerically by calculating the area enclosed by the measured ankle torque–angle curve. This discrepancy is due to the fact that the actual system requires some time (about 50 ms) to output the additional offset torque during the transition from CD to PP. As noted earlier, the main purpose of the target stance phase behavior was to serve as an initial guideline for doing net work at the joint. Thus, it was acceptable to allow the actual response to deviate by a small amount from the target behavior as long as sufficient energy was supplied throughout each gait cycle to power the amputee participant’s gait.

According to Section VI, the foot contact was determined based on both pressure sensors on the foot and the measured ankle joint torque. It was desirable to setup the trigger in a way that the toe-off was triggered before the ankle joint reached the zero torque level (see Fig. 17) because that provided enough time for the control system to switch from impedance control mode to position control mode at the transition from stance to swing.

### B. Metabolic Cost Study

For each of the three experimental conditions, the steady state rate of metabolic energy consumption was determined by first plotting the total cumulative energy versus walking time for each experimental trial. The data typically reached a constant slope after approximately 2 min from the start of the walking trial, indicating that the rate of metabolic energy consumption had reached a steady state value. Sample data are shown in Fig. 18. When using the powered prosthesis with motive power output, the rate of metabolic energy consumption (or average metabolic cost) was the lowest among all other conditions (see Table VI for participant values).

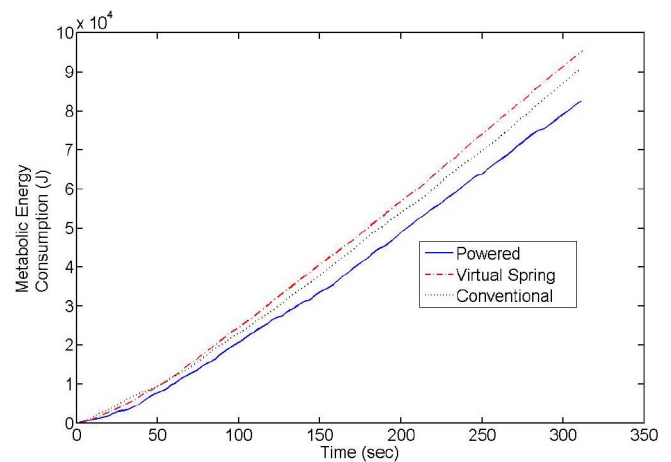


Fig. 18. Metabolic energy consumption of amputee participant 1 walking at a self-selected speed for three conditions: 1) using their conventional passive prostheses (conventional); 2) using the powered prosthesis with only a virtual spring response (virtual spring); and 3) using the powered prosthesis with a nonconservative, motive power output (powered).

The metabolic COT for each participant and experimental condition is shown in Fig. 19. Here again, the metabolic COT when participants used the powered prosthesis with motive power output was the lowest among all experimental conditions. The powered prosthesis with this condition was found to decrease the COT from 7% to 20% compared to the conventional passive-elastic prostheses. The average improvement in the metabolic COT among the participants was 14%. By comparing condition (3) to the virtual spring condition (2), the relative effect of the nonconservative, motive power output was determined. Condition (3) decreased the COT by 7% compared to condition (1) and 16% compared to condition (2), highlighting the benefits of performing net positive work during stance. The results for the metabolic COT study are summarized in Table VI.

In addition to COT, we computed the metabolic energy consumed per distance traveled (joules per meter) for each participant and condition (see Table VI). For all study participants, the powered prosthesis was found to decrease the metabolic energy consumed per distance traveled from 4% to 16% compared to the conventional passive-elastic prostheses.

## IX. DISCUSSIONS

### A. Prosthesis Weight Versus Power Output

Due to the passive nature of conventional prostheses, and their relatively low power output capability, prosthetic designers have sought to keep prosthetic weight much less than that of the human ankle–foot complex in an effort to maximize walking metabolic economy. In this investigation we hypothesize that a powered ankle–foot prosthesis that mimics the mechanical response of the human ankle in walking can decrease the metabolic cost of transport compared to a conventional passive-elastic prosthesis. Our data are in support of this hypothesis. We find that the powered prosthesis improves amputee metabolic COT from 7% to 20% compared to the conventional passive-elastic prostheses evaluated (Flex-Foot Ceterus and Freedom

TABLE VI  
RESULTS OF THE METABOLIC COST STUDY

Results	Participant		
	1	2	3
Walking Speed (m/s)	1.38	1.67	1.67
Stride Period (s)	1.13	1.07	1.1
Net Mechanical Work Per Step (Joules/Step)	19.9	19.0	13.7
Estimated Electrical Energy Consumption Per Step (Joules/step)	29.3	33.4	31.5
Average Metabolic Cost (W) (Conventional)	325	317	415
Average Metabolic Cost (W) (Virtual Spring)	347	304	473
Average Metabolic Cost (W) (Powered)	282	265	401
Metabolic Energy Consumed Per Distance Traveled (Joules/m)(Conventional)	236	190	249
Metabolic Energy Consumed Per Distance Traveled (Joules/m)(Virtual Spring)	251	183	283
Metabolic Energy Consumed Per Distance Traveled (Joules/m) (Powered)	205	159	240
COT (Conventional)	0.26	0.25	0.30
COT (Virtual Spring)	0.27	0.23	0.33
COT (Powered)	0.22	0.20	0.28

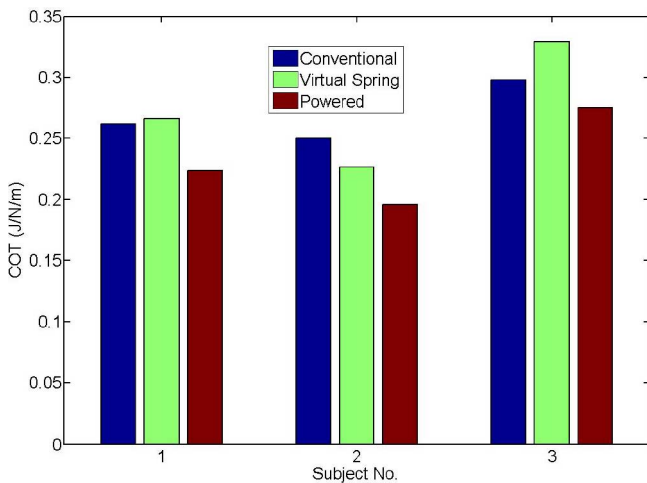


Fig. 19. Metabolic cost of transport for three participants.

Innovations Sierra), even though the powered system is twofold heavier than the conventional devices. This result highlights the fact that prosthesis weight alone is not necessarily a detriment to the clinical performance of a prosthetic intervention. As the results of this investigation suggest, the weight of a powered ankle-foot prosthesis need not hinder an amputee's gait as long as the prosthesis can provide sufficient power output at terminal stance. In addition to the metabolic COT quantitative measurements, amputee participants reported that the powered prosthesis did not feel heavy when the motive power controller was employed (condition 3). They also communicated that the powered prosthesis with the motive power controller made walking easier and less demanding as compared to the conventional prostheses evaluated in the study. However, not surprisingly, the participants reported that the powered prosthesis felt exceedingly heavy when the virtual spring controller was used (condition 2).

### B. Mechanical Design

The results of this investigation highlight the importance of using a parallel spring with a force-controllable actuator comprising series elasticity. To deliver a human-like mechanical

ankle response during the stance period of walking, a prosthetic ankle-foot system requires a high mechanical power output (or a large force bandwidth) as well as a large peak torque. The parallel spring effectively lowers the forces borne by the actuator, and consequently, allows for a higher force bandwidth and a smaller reduction ratio. Series elasticity is also an important design feature as it protects the transmission from shock loads, especially at heel strike. The basic architecture of parallel and series elasticity may also prove useful for other types of assistive devices that require both high power and torque output, such as a hip-actuated orthosis [52].

### C. Self-Selected Walking Speed

As mentioned in Section I, researchers have hypothesized that a powered prosthesis may also increase an amputee's self-selected walking speed [13]–[15]. In this investigation, we found that the self-selected walking speed of participant 2 was increased while the self-selected walking speed for the other two participants remained the same. From these pilot data, it is not clear why self-selected walking speed was not increased for all study participants. Clearly, in future investigations, more comprehensive experiments need to be conducted to further explore the effects of powered plantar flexion on walking speed. Interestingly, for participant 2, when using his conventional passive prosthesis, his self-selected speed was 1.45 m/s, whereas with the powered prosthesis, his self-selected speed was increased to 1.68 m/s, a 16% speed increase. We also measured the COT of participant 2 with his conventional passive prosthesis walking at 1.45 m/s (COT = 0.22). Remarkably, when using the powered ankle-foot prosthesis, not only was this participant's walking speed increased by 16%, but his COT was still 9% lower than when he used his conventional prosthesis at the slower 1.45 m/s speed.

### D. Energetic Requirements of a Powered Ankle-Foot Prosthesis

A powered prosthesis must operate for at least one full day before the user has to recharge the battery. Using step count monitoring systems, researchers have determined that active transtibial amputees walk  $3060 \pm 1890$  steps per day [53]. Assuming the worst case of an amputee walking for 5000 steps at a fast

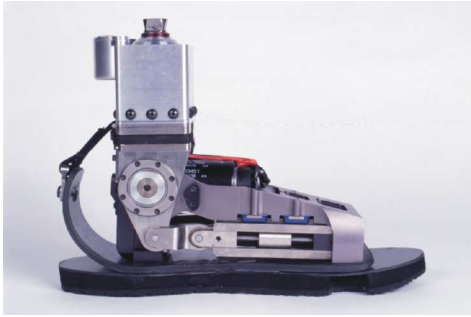


Fig. 20. Compact ankle-foot prosthesis design. The design of the prosthesis fits both human ankle-foot dimensions and geometry, with compact integrated battery and other electronic components onboard.

walking speed while using the powered prosthesis, how large would the onboard battery have to be? Using clinical data from this investigation, the average electrical energy consumption of the motor for each gait cycle was  $31 \pm 2$  J/cycle, with the mean cycle period equal to  $1.10 \pm 0.03$  s. Using a Li-Polymer battery [energy density 165 W·h/kg (see [www.thunderpowercc.com](http://www.thunderpowercc.com))], a 0.24 kg battery would enable 5000 steps of fast powered walking. This battery mass is reasonable, as it is the same size as the required battery for Össur's Proprio Foot [1] now being sold commercially.

To further minimize energy consumption during daily life usage, three control approaches have been implemented in the powered prosthesis. First, the prosthesis was designed to behave as a virtual spring at slow walking speeds (see Section V-C), requiring only a modest level of energy from the battery (2 J/cycle). Second, when the prosthesis is not moving for a given period of time (e.g., when sitting or standing), the prosthesis reverts to a sleep mode, where no current is applied to the motor for actuation. Third, since the human ankle predominantly does negative work during stair descent or walking downhill [54], the powered prosthesis generates electrical power during these activities, converting negative mechanical work at the joint into electrical battery energy as the motor is being backdriven.

In addition to these control approaches, a more viable electromechanical system was recently developed (see Fig. 20). By exploiting high-strength lightweight materials, such as carbon fiber, and a new packaging architecture, the weight of the powered prosthesis was reduced to 1.7 kg (3.8 pounds) including all system components except battery. With a battery attached, the total weight of the system becomes 2 kg, 0.9 kg less than the prototype employed in this investigation (prototype mass = 2.9 kg; see Table IV). Since added prosthetic mass tends to increase the metabolic cost of ambulation, this 0.9 kg reduction may result in an even greater metabolic advantage than the 14% reduction observed in this investigation.

## X. FUTURE WORK

In future investigations, we plan to conduct a comprehensive biomechanical gait study, including the measurement of kinematic and kinetic data. Such an investigation may provide important insights into the biomechanical mechanisms for the

observed metabolic cost reduction. Furthermore, such a study may also provide insight into the optimal control system design of a powered ankle-foot prosthesis.

In addition to level-ground walking, we also plan to study the effect of the powered prosthesis on other daily life activities such as stair and slope ascent/descent gaits. Clearly, for some common activities such as getting in and out of a car, the powered prosthesis may not perform as well as a lightweight conventional prosthesis, since in this particular situation, the added weight of the powered system cannot be compensated for by the active push-off feature. Clearly, additional investigations will be necessary to provide a more comprehensive understanding of the potential advantages and disadvantages of a powered prosthesis. It is our hope that this work will lead to further studies linking prosthetic design to clinical outcomes, resulting in an even wider range of locomotory performance advantages for contemporary prostheses.

## ACKNOWLEDGMENT

The authors would like to thank E. C. Martinez and B. Deffenbaugh for their contributions in mechanical and circuit designs.

## REFERENCES

- [1] Össur, Inc. (2008). [Online]. Available: [www.ossur.com](http://www.ossur.com)
- [2] D. A. Winter, "Biomechanical motor pattern in normal walking," *J. Motor Behav.*, vol. 15, no. 4, pp. 302–330, 1983.
- [3] S. Ron, *Prosthetics and Orthotics: Lower Limb and Spinal*. Baltimore, MD: Williams & Wilkins, 2002.
- [4] N. H. Molen, "Energy/speed relation of below-knee amputees walking on motor-driven treadmill," *Int. Z. Angew. Physiol.*, vol. 31, pp. 173–185, 1973.
- [5] G. R. Colborne, S. Naumann, P. E. Longmuir, and D. Berbrayer, "Analysis of mechanical and metabolic factors in the gait of congenital below knee amputees: A comparison of the SACH and Seattle feet," *Amer. J. Phys. Med. Rehabil.*, vol. 71, no. 5, pp. 272–278, 1992.
- [6] D. A. Winter and S. E. Sienko, "Biomechanics of below-knee amputee gait," *J. Biomech.*, vol. 21, no. 5, pp. 361–367, 1988.
- [7] H. B. Skinner and D. J. Effeney, "Gait analysis in amputees," *Amer. J. Phys. Med.*, vol. 64, pp. 82–89, 1985.
- [8] H. Bateni and S. Olney, "Kinematic and kinetic variations of below-knee amputee gait," *J. Prosthet. Orthot.*, vol. 14, no. 1, pp. 2–13, 2002.
- [9] M. Palmer, "Sagittal plane characterization of normal human ankle function across a range of walking gait speeds," Master's thesis, Dept. Mech. Eng., Massachusetts Inst. Technol., Boston, 2002.
- [10] D. H. Gates, "Characterizing ankle function during stair ascent, descent, and level walking for ankle prosthesis and orthosis design," Master's thesis, Dept. Biomed. Eng., Boston Univ., Boston, MA, 2004.
- [11] A. Hansen, D. Childress, S. Miff, S. Gard, and K. Mesplay, "The human ankle during walking: Implication for the design of biomimetic ankle prosthesis," *J. Biomech.*, vol. 37, no. 10, pp. 1467–1474, 2004.
- [12] A. L. Hof, B. A. Geelen, and J. W. Van Den Berg, "Calf muscle moment, work and efficiency in level walking: role of series elasticity," *J. Biomech.*, vol. 16, no. 7, pp. 523–537, 1983.
- [13] A. D. Kuo, "Energetics of actively powered locomotion using the simplest walking model," *J. Biomech. Eng.*, vol. 124, pp. 113–120, 2002.
- [14] A. D. Kuo, J. M. Donelan, and A. Ruina, "Energetic consequences of walking like an inverted pendulum: Step-to-step transitions," *Exerc. Sport Sci. Rev.*, vol. 33, no. 2, pp. 88–97, 2005.
- [15] A. Ruina, J. E. Bertram, and M. Srinivasan, "A collisional model of the energetic cost of support work qualitatively explains leg sequencing in walking and galloping, pseudo-elastic leg behavior in running and the walk-to-run transition," *J. Theor. Biol.*, vol. 237, no. 2, pp. 170–192, 2005.
- [16] W. Koniuk, "Self-adjusting prosthetic ankle apparatus," U.S. Patent 6 443 993, Sep. 3, 2002.
- [17] C. Li, M. Tokuda, J. Furusho, K. Koyanagi, S. Morimoto, Y. Hashimoto, A. Nakagawa, and Y. Akazawa, "Research and development of the



- intelligently-controlled prosthetic ankle joint," in *Proc. IEEE Int. Conf. Mechatronics Autom.*, Luoyang, China, 2006, pp. 1114–1119.
- [18] A. Hansen, D. Childress, S. Miff, S. Gard, and K. Mesplay, "Automatically-adapting ankle-foot prosthesis concept," presented at the 12th World Congr. Int. Soc. Prosthet. Orthot., Vancouver, BC, Canada, Jul. 2007.
- [19] S. H. Collins and A. D. Kuo, "Controlled energy storage and return prosthesis reduces metabolic cost of walking," in *Proc. ISB XXth Congr. Amer. Soc. Biomech. Annu. Meeting*, Cleveland, OH, Aug. 2003, p. 804.
- [20] G. K. Klute, J. Czerniecki, and B. Hannaford, "Development of powered prosthetic lower limb," presented at the 1st Natl. Meeting, Veterans Affairs Rehabil. R&D Service, Washington, DC, Oct. 1998.
- [21] R. Versluys, L. Peeraer, G. Van der Perre, B. Van Gheluwe, and D. Lefeber, "Design of a powered below-knee prosthesis," presented at the 12th World Congr. Int. Soc. Prosthet. Orthot., Vancouver, BC, Canada, Jul. 2007.
- [22] S. K. Au, P. Bonato, and H. Herr, "An EMG-position controlled system for an active ankle-foot prosthesis: An initial experimental study," in *Proc. IEEE Int. Conf. Rehabil. Robot.*, Chicago, IL, Jun. 2005, pp. 375–379.
- [23] S. K. Au and H. Herr, "Initial experimental study on dynamic interaction between an amputee and a powered ankle-foot prosthesis," presented at the Workshop Dyn. Walking: Mech. Control Hum. Robot Locomotion, Ann Arbor, MI, Jul. 2006.
- [24] S. K. Au, J. Weber, and H. Herr, "Biomechanical design of a powered ankle-foot prosthesis," in *Proc. IEEE Int. Conf. Rehabil. Robot.*, Noordwijk, The Netherlands, Jun. 2007, pp. 298–303.
- [25] S. K. Au, J. Weber, E. Martinez-Villapando, and H. Herr, "Powered ankle-foot prosthesis for the improvement of amputee ambulation," in *Proc. IEEE Int. Conf. Eng. Med. Biol.*, Lyon, France, Aug. 2007, pp. 3020–3026.
- [26] H. Herr, J. Weber, and S. K. Au, "Powered ankle-foot prosthesis," in *Proc. Biomech. Lower Limb Health, Dis. Rehabil.*, Manchester, U.K., Jul. 2007, pp. 72–74.
- [27] S. K. Au and H. Herr, "On the design of a powered ankle-foot prosthesis: The importance of series and parallel motor elasticity," *Robot. Autom. Mag.*, vol. 15, no. 3, pp. 52–59, Sep. 2008.
- [28] S. K. Au, "A powered ankle-foot prosthesis that improves transtibial amputee ambulation," Ph.D. dissertation, Massachusetts Inst. Technol., Cambridge.
- [29] J. Hitt, R. Bellman, M. Holgate, T. Sugar, and K. Hollander, "The sparky (spring ankle with regenerative kinetics) projects: Design and analysis of a robotic transtibial prosthesis with regenerative kinetics," in *Proc. ASME Int. Des. Eng. Tech. Conf.*, Sep. 2007, pp. 1–10, (CD-ROM).
- [30] K. Koganezawa and I. Kato, "Control aspects of artificial leg," in *Proc. IFAC Control Aspects Biomed. Eng.*, 1987, pp. 71–85.
- [31] S. Au, P. Dilworth, and H. Herr, "An ankle-foot emulator system for the study of human walking biomechanics," in *Proc. IEEE Int. Conf. Robot. Autom.*, Orlando, FL, May 2006, pp. 2939–2945.
- [32] K. Hirai, M. Hirose, Y. Haikawa, and T. Takenaka, "The development of Honda humanoid robot," in *Proc. IEEE/RSJ Int. Conf. Intell. Robots Syst.*, Leuven, Belgium, May 1998, pp. 1321–1326.
- [33] K. Kaneko, F. Kanehiro, S. Kajita, H. Hirukawa, T. Kawasaki, M. Hirata, K. Akachi, and T. Isozumi, "Humanoid robot HRP-2," in *Proc. IEEE Int. Conf. Robot. Autom.*, New Orleans, LA, Apr. 2004, pp. 1083–1090.
- [34] D. A. Winter, *Biomechanics and Motor Control of Human Movement*, 2nd ed. New York: Wiley, 1990.
- [35] V. T. Inman, H. J. Ralston, and F. Todd, *Human Walking*. Baltimore, MD: Williams & Wilkins, 1981.
- [36] J. Perry, *Gait Analysis: Normal and Pathological Function*. Thorofare, NJ: Slack, 1992.
- [37] A. R. Tilley, H. Dreyfuss, and S. B. Wilcox, *The Measure of Man and Woman: Human Factors in Design*, Rev. ed. New York: Wiley, 2001.
- [38] G. A. Pratt and M. M. Williamson, "Series elastic actuators," in *Proc. IEEE/RSJ Int. Conf. Intell. Robots Syst.*, Pittsburgh, PA, 1995, pp. 399–406.
- [39] D. Robinson, "Design and an analysis of series elasticity in closed-loop actuator force control," Ph.D. dissertation, Massachusetts Inst. Technol., Cambridge, 2000.
- [40] [Online]. Available: www.maxon.com
- [41] D. L. Grimes, "An active multi-mode above-knee prosthesis controller," Ph.D. dissertation, Massachusetts Inst. Technol., Cambridge, 1976.
- [42] D. Zlatnik, B. Steiner, and G. Schweitzer, "Finite-state control of a transfemoral prosthesis," *IEEE Trans. Control Syst. Technol.*, vol. 10, no. 3, pp. 408–420, May 2002.
- [43] N. Hogan, "Impedance control: An approach to manipulation: Parts I–III," *AMSE J. Dyn. Syst. Meas. Control*, vol. 107, pp. 1–24, 1985.
- [44] N. Hogan and S. P. Buerger, "Impedance and interaction control," in *Robotics and Automation Handbook*, T. R. Kurfess, Ed., Boca Raton, FL: CRC, 2004, ch. 19.
- [45] K. A. Pasch and W. P. Seering, "On the drive systems for high performance machines," *AMSE J. Mech., Transmiss. Autom. Des.*, vol. 106, pp. 102–108, 1984.
- [46] S. D. Eppinger and W. P. Seering, "Three dynamic problems in robot force control," *IEEE Trans. Robot. Autom.*, vol. 8, no. 6, pp. 751–758, Dec. 1992.
- [47] J. E. Colgate, "The control of dynamically interacting systems," Ph.D. dissertation, Massachusetts Inst. Technol., Cambridge, 1998.
- [48] C. T. Johnson and R. D. Lorenz, "Experimental identification of friction and its compensation in precise, position controlled mechanisms," *IEEE Trans. Ind. Appl.*, vol. 28, no. 6, pp. 1392–1398, Dec. 1992.
- [49] [Online]. Available: www.mathworks.com
- [50] C. Hauswirth, A. X. Bigard, and J. M. Lechevelier, "The Cosmed K4 telemetry system as an accurate device for oxygen uptake measurement during exercise," *Int. J. Sports Med.*, vol. 18, pp. 449–453, 1997.
- [51] J. M. Brockway, "Derivation of formulae used to calculate energy expenditure in man," *Hum. Nutr.: Clin. Nutr.*, vol. 41, pp. 463–471, 1987.
- [52] C. J. Walsh, "Biomimetic design of an under-actuated leg exoskeleton for load-carrying augmentation," M.S. thesis, Dept. Mech. Eng., Massachusetts Inst. Technol., Cambridge, 2006.
- [53] J. M. Stepien, S. Cavenett, L. Taylor, and M. Crotty, "Activity levels among lower-limb amputees: Self-report versus step activity monitor," *Arch. Phys. Med. Rehabil.*, vol. 88, no. 7, pp. 896–900, 2007.
- [54] B. J. McFadyen and D. A. Winter, "An integrated biomechanical analysis of normal stair ascent and descent," *J. Biomech.*, vol. 21, no. 9, pp. 733–744, 1988.



**Samuel K. Au** received the B.S. and M.S. degrees from the Department of Automation and Computer-Aided Engineering, Chinese University of Hong Kong, Shatin, Hong Kong, and the Ph.D. degree from the Mechanical Engineering Department, Massachusetts Institute of Technology (MIT), Cambridge.

He is currently a Postdoctoral Associate in the Biomechanics Group, MIT Media Laboratory, MIT. His current research interests include system dynamics, system identification, biomedical signal processing, control, biomechanics, artificial intelligence, robotics, and prosthetics.



**Jeff Weber** received the B.A. degree in industrial design and film production from San Francisco State University, San Francisco, CA, in 1992.

He is working as a Research Engineer for the Biomechanics Laboratory at MIT designing active prosthetics. He is also Co-owner of Meka Robotics LLC, San Francisco, where he designs and builds humanoid robots for research in manipulation and health care. Previously he designed humanoid robots for CSAIL at MIT. His research and design experience includes active prosthetic knees and ankles, compliant actuators, arms, and humanoid hands.



**Hugh Herr** (M'04) received the B.A. degree in physics from Millersville University, Millersville, in 1990, the M.S. degree in mechanical engineering from Massachusetts Institute of Technology (MIT), Cambridge, and the Ph.D. degree in biophysics from Harvard University, Cambridge, MA, in 1998.

He is an Associate Professor at the MIT's Program of Media Arts and Sciences, and the Harvard-MIT Division of Health Sciences and Technology. He has authored or coauthored over 60 technical publications in biomechanics and wearable robotics. His current research interests include the application of principles of biomechanics and neural control to guide the designs of prostheses, orthoses, and exoskeletons.

Dr. Herr was the recipient of the 2007 Heinz Award for Technology, Economy, and Employment.